Published in final edited form as:
J Mod Opt. 2008 November 1; 55(19-20): 3237–3254. doi:10.1080/09500340802168639.

Analytical Capabilities of Coherent Anti-Stokes Raman Scattering Microspectroscopy

Rajan Arora, **Georgi I. Petrov**, and **Vladislav V. Yakovlev***
Department of Physics, University of Wisconsin – Milwaukee, P.O. Box 413, Milwaukee, WI 53201, USA

Abstract

Nonlinear Raman scattering is an emerging spectroscopy technique for non-invasive microscopic imaging. It can produce a fluorescence background free vibrational spectrum from a microscopic volume of a sample providing chemically specific information about its molecular composition. We analyze the ability of nonlinear Raman microspectroscopy to detect low concentrated molecular species and evaluate its applicability to study complex solutions.

Keywords

Raman spectroscopy; microscopy; CARS spectroscopy; biomedical imaging

1. Introduction

Non-invasive microscopic imaging of biological systems remains a key problem in understanding the relationship between structure and function on the cellular and molecular levels. Vibrational spectroscopy is typically considered as one of the most informative, truly non-invasive optical techniques capable of providing valuable information on the structure and function of molecules. Raman spectroscopy and microscopy are particular important, since they can provide sub-micron spatial resolution. Since the first introduction of Raman microscope in 1973 [1], optical and laser technology has made a tremendous step forward. The availability of inexpensive, energy efficient, stable and reliable laser sources together with improved technology for spectral filtering and multichannel detection greatly increased our ability to study inorganic and organic materials in picoliter volumes. Raman confocal systems, which are now widely commercially available, permit rejections out of focus signal, making possible high contrast high resolution non-invasive imaging. However, Raman microscopy is still considered an emerging technique for biological imaging. Despite of the obvious advantages of being very informative and almost nondestructive method of studying biological molecules, classical Raman spectroscopy (spectroscopy, using spontaneous Raman scattering) suffers from a series of limitations, such as a fluorescent background and a low signal level. Thus, fluorescent spectroscopy is often used, when real-time measurements are required [2]. On the other hand, nonlinear Raman spectroscopy, and, in particular, spectroscopy of coherent anti-Stokes Raman scattering (CARS), can resolve most of the problems associated with conventional Raman spectroscopy [3]. Firstly, being a nonlinear optical method of spectroscopy, CARS spectroscopy relies on interaction of high intensity laser pulses. Since the intensity of these pulses is the highest in the focal point of a microscope, CARS spectroscopy potentially offers an excellent discrimination against the out of focus signal. A nonlinear optical

*Email: yakovlev@uwm.edu.

Raman microscope will be an ideal confocal microscope without using an additional aperture [4–5], thus greatly increasing the signal collection efficiency. Secondly, nonlinear Raman spectroscopy provides a way to increase a signal's level by increasing the intensity of incoming pump pulses. For ultrashort (picosecond (i.e. 10^{-12} s) pulses, a signal's level can be as much as several orders of magnitude higher than that for conventional Raman spectroscopy for a given average power of the incident laser beam [3]. Another advantage of CARS spectroscopy is that the detected signal is blue-shifted with respect to the excitation wavelengths, i.e. there is no problem of separating the signal from a fluorescent background. It should be also noted that short-pulse lasers, used for CARS spectroscopy, are naturally designed to study ultrafast processes on a molecular time-scale, thus providing with a unique opportunity to study molecular dynamics (such as protein folding, DNA transformations, etc.) in a real-time (i.e. on the time scale of molecular processes). The last but not least, the light waves in the near-IR are much better suited for penetrating biological tissues, because fewer biological molecules absorb them and because light scattering is less at longer wavelengths. All these features of a Coherent anti-Stokes Raman scattering (CARS), a powerful spectroscopic tool has been used extensively for flame, gas phase, plasma, and combustion diagnostics.

Since its first introduction [6], nonlinear Raman microscopy based on CARS spectroscopy, driven by the progress of ultrafast laser technology, has made a tremendous step forward [7–17] making video-rate vibrational imaging possible [18–19]. However, despite the recent widespread of CARS microscopy and all the remarkable progress made over the past few years, the technique is still considered to be an emerging tool in microscopic imaging due to a number of technical difficulties, such as the complexity of the experimental set-up for CARS microscopy, the high cost associated with lasers and the so-called non-resonant background resulting from a non-specific four-wave mixing process.

The purpose of this report is to understand the limits of nonlinear Raman microspectroscopy, while designing and optimizing the most convenient optical set-up for fast and accurate vibrational spectral analysis from a microscopic volume.

2. CARS microspectroscopy

CARS microspectroscopy is a typical example of hyperspectral microscopy, which aims at obtaining a vibrational spectrum from a microscopic volume of a cell or a tissue for the purpose of chemical analysis. Since molecular composition of a typical cell is rather complicated, the overall vibrational spectrum is composed of many overlapping lines and bands presenting an intrinsic difficult of its analysis. Most of the CARS imaging studies were done in a high-frequency vibrational range where the CARS signal from lipids is exceptionally strong. However, the most interesting from a biochemical perspective is the so-called "fingerprint" region of vibrational frequencies from 500 to 1750 cm^{-1}. The strength of Raman lines is significantly reduced for most of the vibrations in this regions, and a typical concentration of molecular species of interest (mostly, proteins) is not as high as in lipid droplets. This type of imaging presents an apparent challenge for spectroscopists in terms of the detection and analysis of CARS signals.

CARS signal originates from a coherent excitation of vibrational level using a pair of optical pulses, ω_1 ("pump") and ω_2 ("Stokes"), separated by a frequency of this vibrational level, Ω, i.e.

$$\omega_1 - \omega_2 = \Omega \tag{1}$$

The third pulse at frequency ω_3 ("probe") is scattered off the coherently excited vibration to generate the signal at the CARS frequency, ω_{CARS} (see Fig. 1):

$$\omega_{CARS}=\omega_3+\Omega=\omega_3+(\omega_1-\omega_2) \tag{2}$$

CARS signal is a coherent signal, i.e. the phase matching conditions have to be fulfilled in order to achieve the efficient signal generation. Microscopic focusing conditions utilizing a high-numerical-aperture lens significantly relax this restriction, allowing for simultaneous detection of the whole CARS spectrum without any special arrangements [20]. This allows us to make an accurate analysis of the generated CARS signal and to directly compare it with the spontaneous Raman signal.

For a simplicity of analysis, we consider just a single vibrational transition, which is characterized by the Raman cross-section, $\frac{d\sigma}{d\Omega}$, and the line-width, Λ. The interaction volume is defined by the focal spot area, $A=\frac{\pi\omega_0^2}{4}$, and the Rayleigh length, $l_R \cong \frac{\pi\omega_0^2}{2\lambda}$, where ω_0 is the beam waist radius, and λ is the incident wavelength, which is assumed to be approximately equal for all the light waves involved in this nonlinear optical interaction. This leads to the total power of CARS signal to be [20]:

$$p_{CARS} \approx \left(\frac{8\pi c\omega_1\omega_3}{\hbar\omega_2^4}\right)^4\left(\frac{N}{\Gamma}\frac{d\sigma}{d\Omega}\right)^2 p_1p_2p_3, \tag{3}$$

which has to be compared with the power of the spontaneous Raman signal

$$p_{Raman} \approx \Delta\Omega l_R N\frac{d\sigma}{d\Omega}p_3, \tag{4}$$

where N is the concentration of molecules, p_i is the incident power for the i-th frequency of the incident wave, and $\Delta\Omega$ is the collection angle for Raman microscopy. Most of the arguments for CARS microscopy are based on the direct comparison of Eqs. (3–4), which leads to the conclusion that for concentrated molecular species and high-power laser sources ($p_i > 10^3 W$) CARS signal is many orders of magnitude stronger than Raman signal. However, the reality is more complicated, when this analysis, which was originally developed for diagnostics of gaseous systems, is applied to biochemical imaging.

The very first important point we would like to make is related to the acceptable level of the incident power. Biological systems are not used to the high-intensity laser irradiation and impose a limit on the maximum incident intensity to be used without the induced cell damage. There is an ongoing debate on what the limiting intensity is for different incident excitation wavelengths, pulse durations, etc. [21–24]; however, it is more or less accepted that the heating effects due to a linear absorption in the near-IR are rather insignificant [24], and the major contribution to the cell damage is coming from the multiphoton absorption [21–23], which can be considerably reduced by implementing excitation sources with the laser wavelength from 900 to 1300 nm [21–23]. This allows using more than an order of magnitude higher incident laser powers, as compared to 800-nm excitation.

The second important aspect of a fair comparison of nonlinear Raman microscopy and microscopy of spontaneous Raman scattering is related to evaluation of their signal-to-noise ratios, as it was first demonstrated in Refs. [25–26]. Here, we simplify the analysis by assuming that highly stable laser sources are used and all the detectors are quantum limited, i.e. the only source of noise is the shot-noise. Both the laser and detection technologies made a significant step forward over the past 30 years making the above assumption quite reasonable. Using Eqs. (3–4) and the procedure described in Ref. [26], we can express the gain in the signal-to-noise ratio (SNR) for CARS spectroscopy with respect to spontaneous Raman spectroscopy as:

$$\frac{SNR_{CARS}}{SNR_{Raman}} \cong 50 \times \left(\frac{p_1}{kW}\right) \times \left(\frac{c}{1M}\right)^{1/2} \times \left(\frac{10cm^{-1}}{\Gamma}\right) \times \left(\frac{d\sigma}{d\Omega} \cdot \frac{1}{10^{-30}cm^2}\right)^{1/2} \times \left(\frac{\lambda_1}{1\mu m}\right)^{3/2} \quad (5)$$

In deriving Eq. (5) we assumed that $p_1 = p_2$, and $\omega_1 \cong \omega_2 \cong \omega_3$, and expressed the concentration of molecules of interest in terms of the molar concentration, c, which is more convenient for biochemical analysis. Eq. (5) provides with a simple way of evaluating a possible use of CARS microspectroscopy. A typical value for the Raman cross-section in the fingerprint region is $\frac{d\sigma}{d\Omega} \cong 10^{-30} cm^2$, typical linewidth is $\Lambda \cong 10\ cm^{-1}$. If one can afford using the incident power of $p_1 \cong 10\ kW$, which should be possible for the excitation wavelength longer than $1\mu m$, the resulted gain in the SNR will be a factor of 50 for the molecular concentration of c=10 mM, which is considered to be rather high for most of the biological molecules. Since the SNR is scaled as a square root of the acquisition time, the total gain in the speed of recording CARS spectra is 2,500 making CARS microspectroscopy extremely attractive. On the other hand, if the excitation wavelength is around 800-nm, biological structures demand the use of the lower power excitation sources, and for the same experimental setting CARS microspectroscopy does not have any advantage with respect to spontaneous Raman spectroscopy.

The above formula does not take into account the fluorescence background, which is common problem for Raman spectroscopy. This background reduces the SNR for Raman measurements [27] by a factor of

$$\frac{SNR_{with\ fluorescence}}{SNR_{w/o\ fluorescence}} = \sqrt{\frac{p_{fluoresence}}{p_{Raman}}}, \quad (6)$$

where $p_{fluorescence}$ is the fluorescence signal from the same volume. This is not the only factor, which is missing in Eq. (5). CARS signal also suffers from a background, which originates from a non-chemically-specific four-wave mixing, which is considered to be one of the most prominent problems of CARS spectroscopy. The presence of this background reduces the SNR for CARS measurements [20,26] by a factor of

$$\frac{SNR_{NR+R}}{SNR_R} = \sqrt{\frac{p_{NR}}{p_R}}, \quad (7)$$

where p_{NR}, p_R are the generated non-resonant and resonant powers of the CARS signal. While water molecules have a relatively low non-resonant Raman cross-section, their concentration in solution is so high that the resonant contribution to the CARS signal is hardly noticeable if the concentration of molecular species of interest is smaller than 100 mM and no measures to reduce this background are taken. We will discuss this issue separately, since it is the primary

challenge in obtaining high-quality CARS spectral data, but, for now, we just assume that this background is not a problem, and Eq. (5) is the only fundamental limit imposed on CARS microspectroscopy. Most of molecular species, e.g. proteins, are rarely occurring in a cell in concentrations higher than 1 mM and have a moderate Raman cross-section in the fingerprint region. Earlier, we demonstrated that the use of the incident beams with a power in excess of 10 kW is essential to achieve significant SNR improvement of CARS spectra measurements. Since the incident light intensity is the major limiting factor, one has to evaluate the experimental conditions, which will allow the use of such high peak powers for cellular imaging. Recently, we did some systematic studies on cell and tissue damage using short-pulsed laser irradiation in the wavelength region around 1000 nm [28]. While, the damage threshold somewhat varies for different cells and tissues, it can be approximately interpolated with a rather simple expression

$$I_{\max} \cong 1.5 \cdot 10^{11} W/cm^2 \sqrt{\frac{1ps}{\tau_p}}, \tag{8}$$

where τ_p is the incident pulse duration of the light wave, which coherently excites molecular vibration. Using Eq. (8) as a guideline, one can see that, if the goal is to achieve microscopic spatial resolution, i.e. $\omega_0 \cong 0.5\mu m$, the maximum allowed incident power is somewhat around $p_1 \cong 200W$ for the incident pulse duration of $\tau_p = 4\,ps$. Clearly, for microscopic imaging of low concentrated ($c \cong 1mM$) molecular species, Raman microscopy does a much better job. CARS microscopy is still providing better SNR even at the highest possible spatial resolution, when used with higher concentrated molecular species and strong Raman transitions (vibrational imaging of lipid distribution using CH_2 stretch vibration provides one of the best examples of such application [29]). For the most general case, one has to increase the incident beam diameter in order to accommodate higher incident power. Indeed, if the beam diameter is increased to about $\omega_0 \cong 3\mu m$, which roughly corresponds to a typical cell, the incident power can be increased to about $p_1 \cong 10\,kW$, making CARS spectral measurements highly favorable.

3. Non-resonant background in CARS microspectroscopy

The non-resonant background in CARS spectroscopy was always considered as one of the biggest challenges to deployment of this spectroscopic technique for analytical measurements. In brief, a non-resonant contribution to the nonlinear optical polarization from surrounding molecules interferes with a resonant contribution producing an overall signal, which has complex frequency dependence. The resulted line shape is given by the following equation:

$$R(\omega) \propto \left|\chi_{NR}^{(3)} + \sum_r \frac{A_r}{\omega_r - \omega - i\Gamma_r}\right|^2, \tag{9}$$

where A_r, ω_r, and Λ_r are the amplitude, the transition frequency, and the linewidth, respectively of the r-th Raman mode. The first term in Eq. (9) is the non-resonant susceptibility, which is considered to be frequency independent. The second term in Eq. (9) corresponds to the resonant contribution. If it is set to zero, the total signal will be just proportional to

$$\left|\chi_R^{(3)}\right|^2 = \left|\sum_r \frac{A_r}{\omega_r - \omega - i\Gamma_r}\right|^2, \tag{10}$$

which is different from the spectral shape of a typical Raman spectrum taken for the same excitation wavelength and defined by

$$|\mathrm{Im}\chi_R^{(3)}|^2=|\mathrm{Im}\sum_r \frac{A_r}{\omega_r-\omega-i\Gamma_r}|^2 \tag{11}$$

Ideally, we want to retrieve the Raman spectrum, which would allow us to directly compare the experimentally measured spectral data with the Raman spectra. There are several ways of dealing with this problem.

a) Polarization suppression

The idea of using polarization properties of $\chi^{(3)}$ tensor to suppress the non-resonant contribution was first suggested and experimentally demonstrated by Akhmanov et al [31]. Later, Shen et al modified the earlier proposed ellipsometric technique to achieve either direct suppression of non-resonant background, or to use this non-resonant background for heterodyne mixing with the resonant contribution to extract either the real or imaginary part of the resonant susceptibility tensor $\chi_R^{(3)}$. Both approaches provide with a substantial non-resonant background suppression, which is limited by the degree of depolarization introduced by a high-numerical-aperture optics and the quality of broadband polarization components. Using polarization preserving microscope objectives and specially selected polarizers and Fresnel rhombs for polarization rotation, we routinely achieved two-three orders of magnitude suppression of the non-resonant background (see Fig. 2). The problem comes, however, when a scattering medium is introduced in the focal plane, which can be, for example, a cell, an organelle, or a piece of tissue. The efficiency of the background suppression is substantially degraded. It gets even worse for a typical tissue imaging, when the whole signal collected in the back-reflected geometry is produced through the light scattering. An additional disadvantage of polarization technique is that the useful signal in all configurations is also reduced.

b) Heterodyne detection

Heterodyne detection is widely used to improve the SNR of optical measurements. The additional advantage of heterodyne detection for CARS measurements is that it allows direct extraction of either real or imaginary part of the susceptibility tensor [33–34]. Being introduced for CARS spectroscopy about 30 years ago [26], heterodyne detection was for a long time considered as the best way of achieving the best SNR in CARS measurements [20,26]. It has been recently adapted for broadband spectral measurements [35]; however, it still suffers from a light scattering in a sample, which affects the phase properties of the signal. It is also hardly applicable for the epi-detection geometry, which is highly desirable for many biomedical applications.

c) Time-delayed methods

The non-resonant background in CARS spectroscopy originates from instantaneous four-mixing processes, while the resonant contribution involves real vibrational states. This provides a basis for a possible discrimination against the non-resonant background. To do so, one has to come up with a pair of pulses, which excite the vibrational state, and the third, time-delayed pulse will only contribute to the resonant part of the CARS signal. However, to make this scheme work efficiently, one has to overcome certain obstacles. To achieve high spectral resolution, the bandwidth of the third pulse should be of the order or less than the linewidth of the Raman line, Λ, which requires the pulse duration of the third pulse to be longer than Λ^{-1}. On the other hand, Λ^{-1} roughly corresponds to the lifetime on the excited state, i.e., if the time

delay is longer than Λ^{-1}, it will substantially degrade the amplitude of the resonance CARS signal. One of the possible solutions to this problem is to use a pair of time-overlapping short pulses to excite the transition and to use a longer probe pulse to scatter off the coherent excitation. This situation is illustrated in Fig. 3. The time-overlap of excitation and probe pulses, i.e. the amplitude of the non-resonant contribution, is approximately proportional to the pulse duration of the excitation pulse(s), while the amplitude of the resonant contribution is roughly proportional to the pulse duration of the probe pulse. One can further suppress the overlap through some pulse shaping techniques, as it was suggested by Scully et al [36]. In this approach, the probe pulse is passed through a spectral filter to produce a square-shaped spectrum, which in a time domain corresponds to the pulse, whose intensity profiles looks like

$$I(t) \propto \left(\frac{\sin t}{t}\right)^2.$$

By making the excitation pulses overlap with the minimum of the probe pulse preceding its main maximum, the non-resonant background is further suppressed [36]. The same idea can be exploited with a single pulse excitation [37], when both pump pulses at requencies ω_1, ω_2 are derived from a single ultrabroadband pulse.

The great advantage of using time-delayed methods to reduce the non-resonant background is that they can work in highly scattering media and can be utilized for biomedical diagnostics of cells and tissues. The obscure disadvantage of this approach is the reduced amplitude of the CARS signal. Indeed, the amplitude of the resonant CARS signal is proportion to the energies of each of the excitation pulses [19,37], the employment of shorter incident pulses in all the proposed schemes requires the downscaling of the input energy as a square root of the pulse duration and, thus, the diminution of the overall signal.

d) Phase retrieval algorithms

The spectral lineshape in CARS spectroscopy is described by Eq. (9). In order to investigate an unknown sample, one needs to extract the imaginary part of $\chi_R^{(3)}$ to be able to compare it with the known spontaneous Raman spectrum. To do so, one has to determine the phase of the resonant contribution with respect to the non-resonant one. This is a well known problem of phase retrieval, which has been discussed in details elsewhere [38]. The basic idea is to use the whole CARS spectrum and the fact that the non-resonant background is approximately constant. The later assumption is justified, if there are no two-photon resonances in the molecular system [26]. There are several approaches to retrieve the unknown phase [38], but the majority of those techniques are based on an iterative procedure, which often converges only for simple spectra and for negligible noise. When dealing with real experimental data, such iterative procedures often fail to reproduce the spectroscopic data obtained by some other means.

The alternative approach is based on a non-iterative procedure utilizing the maximum entropy model (MEM) to extract the complex dielectric susceptibility $\chi_R^{(3)}$ from the intensity measurements. This technique was first proposed 15 years ago [39], and recently was used for multiplexed CARS measurements [13,40].

The concept behind the Maximum Entropy Model is to choose the spectrum in the form of a non-negative function of frequency, which corresponds to a time series with maximum entropy whose autocorrelation function is consistent with the set of known values.

The experimentally measured CARS signal is given by

$$I_{CARS}(\tilde{\omega}_1 - \tilde{\omega}_2) \propto |\chi^{(3)}(\tilde{\omega}_1 - \tilde{\omega}_2)|^2 \tag{12}$$

and is measured with in frequency interval of $\tilde{\omega}_1 \leq \tilde{\omega} \leq \tilde{\omega}_2$. Let us assume that the real and imaginary parts of $\chi^{(3)}(\tilde{\omega}_1 - \tilde{\omega}_2)$ do not change sign in that frequency range and the non-resonant χ_{NR} is real and doesn't depend on frequency. We define a normalized frequency as

$$\nu = \frac{\tilde{\omega} - \tilde{\omega}_1}{\tilde{\omega}_2 - \tilde{\omega}_1} \tag{13}$$

The maximum entropy model estimate for $|\chi(\nu)|^2$ can be written as

$$|\chi^{(3)}(\nu)|^2 = \frac{|\beta|^2}{\left|1 + \sum_{n=1}^{M} a_n \exp(-i2\pi n\nu)\right|^2} \tag{14}$$

where the unknown maximum entropy model coefficient a_n and $|\beta|^2$are functions of estimated autocorrelation C_m. Those MEM coefficients can be found by solving a set of linear equations

$$\begin{pmatrix} C_0 & C_{-1} & \dots & C_{-M} \\ C_1 & C_0 & \dots & C_{1-M} \\ \dots & \dots & \dots & \dots \\ C_M & C_{M-1} & \dots & C_0 \end{pmatrix} \begin{pmatrix} 1 \\ a_1 \\ \dots \\ a_M \end{pmatrix} = \begin{pmatrix} |\beta|^2 \\ 0 \\ \dots \\ 0 \end{pmatrix} \tag{15}$$

where C_m are the Fourier coefficients of signal $|\chi^{(3)}(\nu)|^2$ and are defined as

$$C_m = \int_0^1 |\chi^{(3)}(\nu)|^2 \exp(i2\pi m\nu) d\nu, \quad m \leq M$$

For discrete set of normalized frequencies

$$C_m = \frac{1}{K} \sum_{j=0}^{K-1} |\chi^{(3)}|^2 \exp\left(\frac{i2\pi m j}{K}\right), \quad m \leq M, M \leq \frac{K}{2}$$

Solution to the above *M–th* order equation always exists if the *M*+1 by *M*+1 Toeplitz matrix has a non negative definite. In a typical experimental situation $|\mathrm{Im}\chi_R^{(3)}| \ll |\chi_{NR}^{(3)} + \mathrm{Re}\chi_R^{(3)}|$, i.e. the non-resonant contribution dominates the CARS signal, and the Raman line shape can be calculated using a simple expression:

$$\mathrm{Im}\chi_R^{(3)}(\nu)=\sqrt{\chi^{(3)}(\nu)}\sin\theta(\nu) \tag{16}$$

where $\theta(\nu)$ is the MEM's phase defined as

$$\theta(\nu)=\arg\left[1+\sum_{n=1}^{M}a_n\exp(-i2\pi n\nu)\right].$$

The above procedure of the Raman spectrum retrieval exhibits an amazing robustness with respect to the noise of the data; however, several empirically deduced conditions have to be satisfied for an accurate retrieval. Firstly, the retrieved spectrum is always distorted on the edges, and, to get a good precision, the CARS spectrum has to be taken in a very broad range (see, for example, Fig. 4). Secondly, the presence of strong Raman lines, for which the above assumption of $|\mathrm{Im}\chi_R^{(3)}| \ll |\chi_{NR}^{(3)}+\mathrm{Re}\chi_R^{(3)}|$ is not fulfilled, might affect the retrieved amplitude and shape of this particular line, i.e. the developed algorithm works the best for relatively weak Raman lines. This is really important for CARS measurements. It appears that it is not necessary to attenuate the non-resonant background to complete extinction: some of the residual background helps increasing the signal amplitude. The additional surprising advantage of this approach is that it allows, unlike spontaneous Raman measurements, direct concentration measurements in solution. Indeed, the non-resonant background is predominantly due to the abundance of water molecules, whose concentration for most of the practical applications remains fixed. Thus, the ratio of the resonant signal to the non-resonant background provides with a reliable measure of the relative concentration of molecules under study. Finally, we find that good agreement with independently measured Raman spectra is only possible if a proper normalization of CARS signals is performed. To do so, we typically place a distilled water solution in the place of the sample and collect the reference CARS spectrum. This spectrum contains the convoluted information about the spectral transmission of optical filters and spectrometer, the spectra response of a CCD detector, and the spatial, wavelength-dependent overlap of all the incident beams in the focal plane.

4. Experimental set-up for broadband CARS microspectroscopy

The concept of a broadband CARS microspectroscopy was first introduced in 2000 [41], and was further developed over the past few years [13,23,42–43]. The major idea is to develop a simple CARS microspectrometer, which allows simultaneous recording of the whole vibrational spectrum. This concept is schematically presented in Fig. 5. In the initial design (see Fig. 5), a fundamental of high-energy, mode-locked Nd:YVO_4 oscillator [44–45] was used to serve both as a pump and probe pulse, while the broadband continuum generated in a GeO_2 fiber was utilized as a broadband Stokes pulse. High spectra density generated through the process of stimulated Raman scattering in GeO_2 fiber [42,45] allows fast CARS spectral recording in the spectral range from 200 to 3000 cm^{-1}. Phase retrieval methodology was successfully adapted for CARS signal retrieval. Figures 6–8 illustrate the successful retrieval for several complex systems, which show congested Raman lines in the fingerprint region. Clearly, the described approach works for variety of molecular systems and is capable of reproducing Raman spectra at much faster acquisition rate.

The major challenge is to improve the sensitivity of CARS microspectroscopy, which requires substantial increase of the signal and reduction of the non-resonant background. This can be achieved in a slightly modified setting, when the high-energy continuum generated in an optical

fiber is compressed. While getting a transform-limited pulse is rather difficult, if possible, we can use a pre-compressed pulse, which can be as short as 50–70 fs. It is still two orders of magnitude shorter than the probe pulse and can be used for efficient vibrational excitation [11–12] and the non-resonant background suppression [19]. The later is illustrated in the following example of glucose sensing using CARS microspectroscopy. In this particular example, a relatively low concentrated solution of glucose shows a reproducible CARS signal (see Fig. 9a), which is later retrieved using the described above algorithm (see Fig. 9b). An excellent agreement with the independently recorded Raman spectrum demonstrates the great promise of CARS microspectroscopy for non-invasive glucose concentration measurements.

5. Conclusion

CARS microspectroscopy is a promising emerging techniquel for non-invasive biomedical imaging. The developments in laser spectroscopy over the past few years made real-time measurements possible and allowed significant suppression of the non-resonant background. Through the development of the phase retrieval algorithm, the direct comparison of CARS and Raman measurements becomes possible. The deployment of the CARS retrieval strategy with partially suppressed non-resonant background allows for the relative concentration measurements of molecular species of interest. In the same time, there are some limitations of CARS microspectroscopy, which are mostly related to imaging on a submicroscopic scale of low concentrated molecular species. However, there are many important applications such as glucose concentration measurements, cell cytometry, microfluidic diagnostics, etc., where CARS microspectroscopy can be an indispensable tool for express chemical analysis.

Acknowledgments

This work was partially supported by the NSF grant ECS-9984225, the NIH Grant R21RR14257 and the University of Wisconsin Milwaukee RGI grant.

References

1. Hirschfeld T. Raman microprobe: vibrational spectroscopy in the femtogram range. J Opt Soc Am 1973;63:476–483.
2. Lakowicz, JR. Principles of fluorescent spectroscopy. Plenum Press; New York: 1983.
3. Hudson BS. New laser techniques for biophysical studies. Ann Rev of Biophys Bioengin 1977;6:135–150.
4. Wilson, T. Confocal microscopy. Academic Press; London: 1990.
5. Denk W, Strickler JH, Webb WW. Two-photon laser scanning fluorescence microscopy. Science 1990;248:73–76. [PubMed: 2321027]
6. Duncan MD, Reintjes J, Manuccia TJ. Scanning coherent anti-Stokes Raman microscope. Opt Lett 1982;7:350–352. [PubMed: 19714017]
7. Zumbusch A, Holton GR, Xie XS. Three-dimensional vibrational imaging by coherent anti-Stokes Raman scattering. Phys Rev Lett 1999;82:4142–4145.
8. Potma EO, de Boeij WP, van Haastert PJM, Wiersma DA. Real-time visualization of intracellular hydrodynamics in single living cells. Proc Natl Acad Sci 2001;98:1577–1582. [PubMed: 11171993]
9. Hashimoto M, Araki T. Molecular vibration imaging in the fingerprint region by use of coherent anti-Stokes Raman scattering microscopy with a collinear configuration. Opt Lett 2000;25:1768–1770. [PubMed: 18066338]
10. Wurpel GWH, Schins JM, Muller M. Chemical specificity in three-dimensional imaging with multiplex coherent anti-Stokes Raman scattering microscopy. Opt Lett 2002;27:1093–1095. [PubMed: 18026371]
11. Dudovich N, Oron D, Silberberg Y. Single-pulse coherently controlled nonlinear Raman spectroscopy and microscopy. Nature 2002;418:512–514. [PubMed: 12152073]

12. Lim SH, Gaster AG, Leone SR. Single-pulse coherently controlled nonlinear Raman scattering spectroscopy. Phys Rev A 2005;72:0418031.

13. Petrov GI, Arora R, Yakovlev VV, Wang X, Sokolov AV, Scully MO. Comparison of coherent and spontaneous Raman microspectroscopies for noninvasive detection of single bacterial endospores. Proc Natl Acad Sci USA 2007;104:7776–7779. [PubMed: 17483468]

14. Konorov SO, Glover CH, Piret JM, Bryan J, Schulze HG, Blades MW, Turner RFB. In situ analysis of living embryonic cells by coherent anti-Stokes Raman microscopy. Anal Chem 2007;79:7221–7225. [PubMed: 17691751]

15. Kano H, Hamaguchi HO. Supercontinuum dynamically visualizes a dividing single cell. Anal Chem 2007;79:8967–8973. [PubMed: 17966989]

16. Lozovoy VV, Dantus M. Coherent control in femtochemistry. Chem Phys Chem 2005;6:1970–2000. [PubMed: 16208734]

17. von Vocano B, Motzkus M. Time-resolved two color single-beam CARS employing supercontinuum and femtosecond pulse shaping. Opt Commun 2006;264:488–493.

18. Evans CL, Potma EO, Puorishaag M, Cote D, Lin CP, Xie XS. Chemical imaging of tissue in vivo with vide rate coherent anti-Stokes Raman scattering microscopy. Proc Natl Acad Sci USA 2005;102:16807–16812. [PubMed: 16263923]

19. Pestov D, Wang X, Ariunbold GO, Murawski RK, Sautenkov VA, Dogariu A, Sokolov AV, Scully MO. Single-shot detection of bacterial endospores via coherent Raman spectroscopy. Proc Natl Acad Sci USA 2008;105:422–427. [PubMed: 18184801]

20. Akhmanov, SA.; Koroteev, NI. Methods of nonlinear optics in light scattering. Moscow: Nauka; 1981.

21. Squirrell JM, Wokosin DL, White JG, Bavister BD. Long-term two-photon fluorescence imaging of mammalian embryos without compromising viability. Nat Biotechnol 1999;17:763–767. [PubMed: 10429240]

22. Konig K, Becker TW, Fischer P, Riemann I, Halbhuber KJ. Pulse-length dependence of cellular response to intense near-infrared laser pulses in multiphoton microscopes. Opt Lett 1999;24:113–115. [PubMed: 18071425]

23. Yakovlev VV. Advanced instrumentation for non-linear Raman microscopy. J Raman Spectr 2003;34:957–964.

24. Schonle A, Hell SW. Heating by absorption in the focus of an objective lens. Opt Lett 1998;23:325–327. [PubMed: 18084500]

25. Tolles WM, Turner RD. A comparative analysis of the analytical capabilities of coherent antistokes Raman spectroscopy (CARS) relative to Raman scattering and absorption spectroscopy. Appl Spectrosc 1977;31:96–103.

26. Eesley GL, Levenson MD, Tolles WM. Optically heterodyned coherent Raman spectroscopy. IEEE J Quant Electron 1978;14:45–49.

27. Yakovlev VV. Time-gated confocal Raman microscopy. Spectroscopy 2007;22:34–41.

28. Yakovlev VV, Noojin G, Denton M, Thomas RJ. Real-time monitoring of chemical and structural changes induced by ultrashort pulse interactions with tissues and cells. SPIE Proceedings 2008;6859:685914.

29. Hellerer T, Axang C, Brackmann C, Hillertz P, Pilon M, Enejder A. Monitoring lipid storage in Caenorhabditis elegans using coherent anti-Stokes Raman scattering microscopy. Proc Natl Acad Sci USA 2007;104:14658–14663. [PubMed: 17804796]

30. Volkmer A. Vibrational imaging and microspectroscopies based on coherent anti-Stokes Raman scattering microscopy. J Phys D 2005;38:R59–R81.

31. Akhmanov SA, Bunkin AF, Ivanov SG, Koroteev NI. Coherent ellipsometry of Raman scattering of light. JETP Lett 1977;25:444–449.

32. Oudar JL, Smith RW, Shen YR. Polarization-sensitive coherent anti-Stokes Raman spectroscopy. Appl Phys Lett 1979;34:758–760.

33. Vinergoni C, Bredfeldt JS, Marks DL, Boppart SA. Nonlinear optical contrast enhancement for optical coherence tomography. Opt Express 2004;12:3310341.

34. Evans CL, Potma EO, Xie XSN. Coherent anti-Stokes Raman scattering spectral interferometry: determination of the real and imaginary components of nonlinear susceptibility $\chi^{(3)}$ for vibrational microscopy. Opt Lett 2004;29:2923–2925. [PubMed: 15645825]
35. Kee TW, Zhao HX, Cicerone MT. One-laser interferometric broadband coherent anti-Stokes Raman scattering. Opt Express 2006;14:3631–3640. [PubMed: 19516510]
36. Pestov D, Murawski RK, Aribunbold GO, Wang X, Zhi MC, Sokolov AV, Sautenkov VA, Rostovtsev YV, Dogairu A, Huang Y, Scully MO. Optimizing the laser-pulse configuration for coherent Raman spectroscopy. Science 2007;316:265–268. [PubMed: 17431177]
37. Dudovich N, Oron D, Silberberg Y. Single-pulse coherent anti-Stokes Raman spectroscopy in the fingerprint spectral region. J Chem Phys 2003;118:9208–9215.
38. Lucarini, V.; Saarinen, JJ.; Peiponen, K-E.; Vartiainen, EM. Kramers-Kronig relations in optical material research. Springer; Berlin: 2005.
39. Vartiainen EM. Phase retrieval approach for coherent anti-Stokes Raman scattering spectrum analysis. J Opt Soc Am B 1992;9:1209–1214.
40. Vartiainen EM, Rinia HA, Muller M, Bonn M. Direct extraction of Raman line-shapes from congested CARS spectra. Opt Express 2006;14:3622–3630. [PubMed: 19516509]
41. Yakovlev VV. Advances in real-time nonlinear Raman microscopy. Proceedings of SPIE: Biomedical Diagnostic, Guidance, and Surgical-Assist Systems III 2001;4254:97–105.
42. Petrov GI, Yakovlev VV. Enhancing red-shifted white-light continuum generation in optical fibers for applications in nonlinear Raman microscopy. Opt Express 2005;13:1299–1306. [PubMed: 19495003]
43. Petrov GI, Yakovlev VV, Sokolov A, Scully MO. Detection of Bacillus subtilis spores in water by means of broadband coherent anti-Stokes Raman spectroscopy. Opt Express 2005;13:9537–9542. [PubMed: 19503156]
44. Petrov GI, Yakovlev VV, Minkovski NI. Broadband nonlinear optical conversion of a high-energy diode-pumped picosecond laser. Opt Commun 2004;229:441–445.
45. Petrov GI, Yakovlev VV, Minkovski NI. Near-infrared continuum generation of femtosecond and picosecond pulses in doped optical fibers. Appl Phys B 2003;77:219–225.

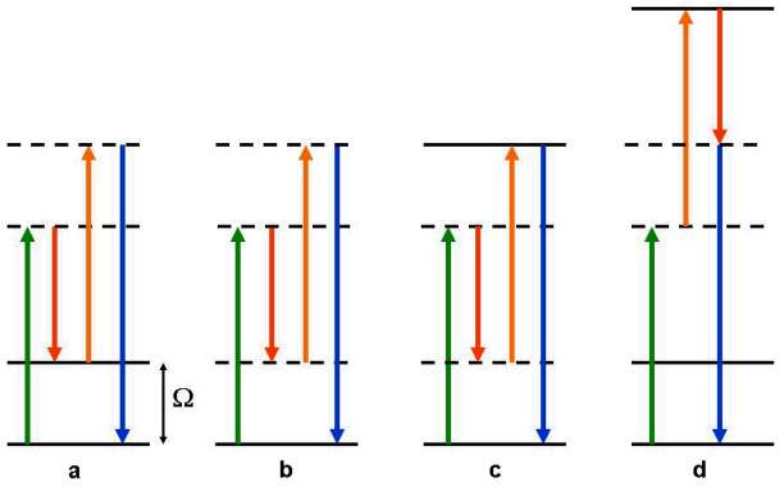

Figure 1.

Diagram of various four-wave mixing processes resulting in generation of $\omega_{CARS} = \omega_3 + (\omega_1 - \omega_2)$: a) resonant CARS process, involving coherent excitation of a vibrational state (shown as a solid line), b) non-resonant CARS process, involving transitions only through virtual states (shown as dashed lines), c–d) different non-resonant CARS processes, which do not involve excitation of vibrational states, but involve electronic state transitions.

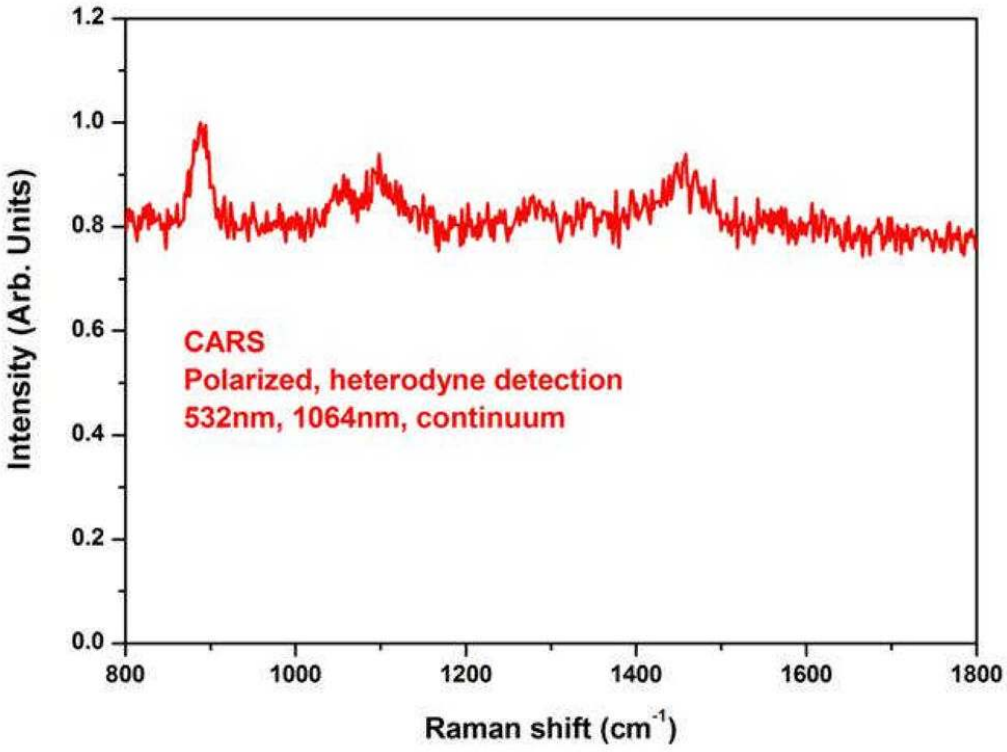

Figure 2.
Vibrational spectrum from 5% (volume) ethanol solution in water. Experimentally measured heterodyne CARS spectrum (see [32] for more details).

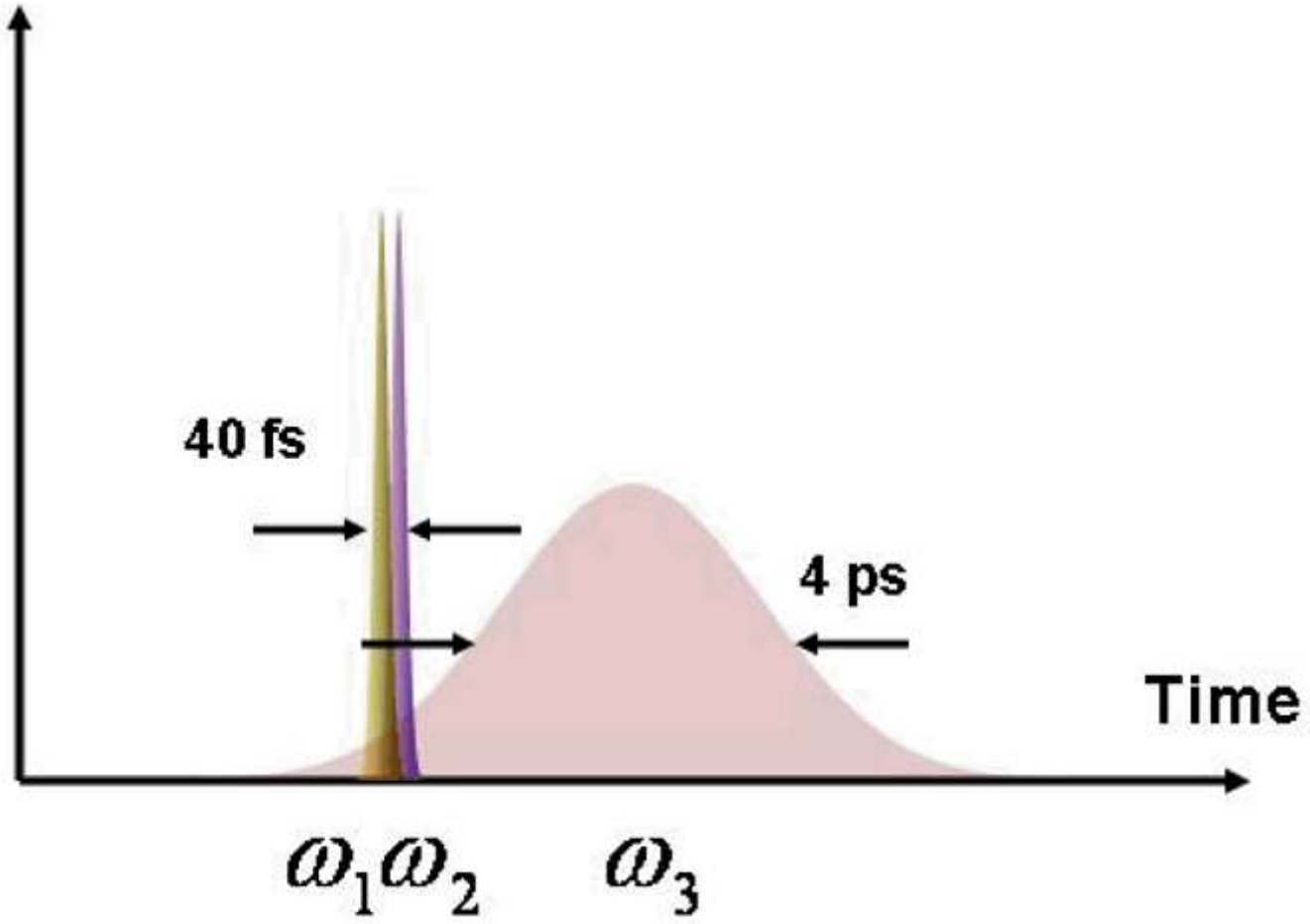

Figure 3.
Temporal arrangement of three incident pulses, which requires two ultrashort pulses ("pump" and "Stokes") to be temporally overlapped and preceding the peak of the third (long) pulse.

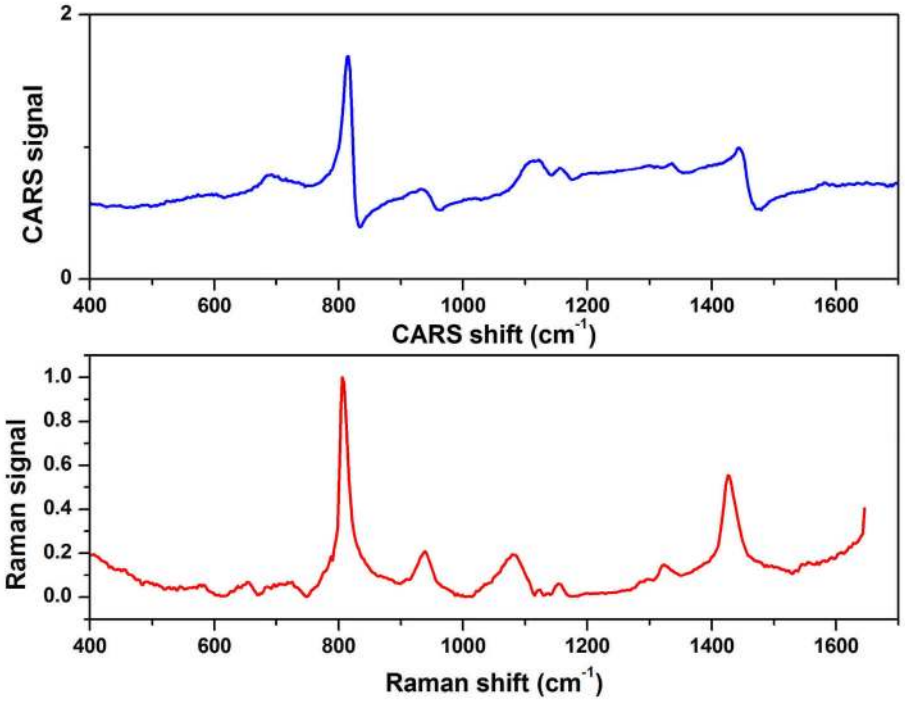

Figure 4.
Top panel: experimentally measured CARS spectrum from an isopropyl solution. Bottom panel: Raman spectrum retrieved from the CARS spectrum.

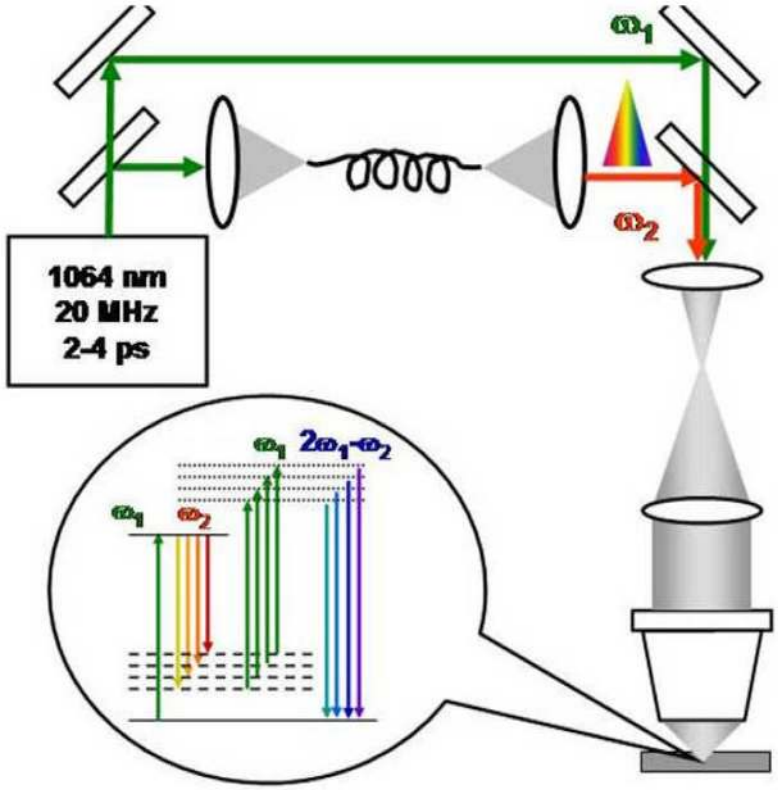

Figure 5.
Schematic diagram illustrating the concept of ultrabroadband CARS microspectroscopy.

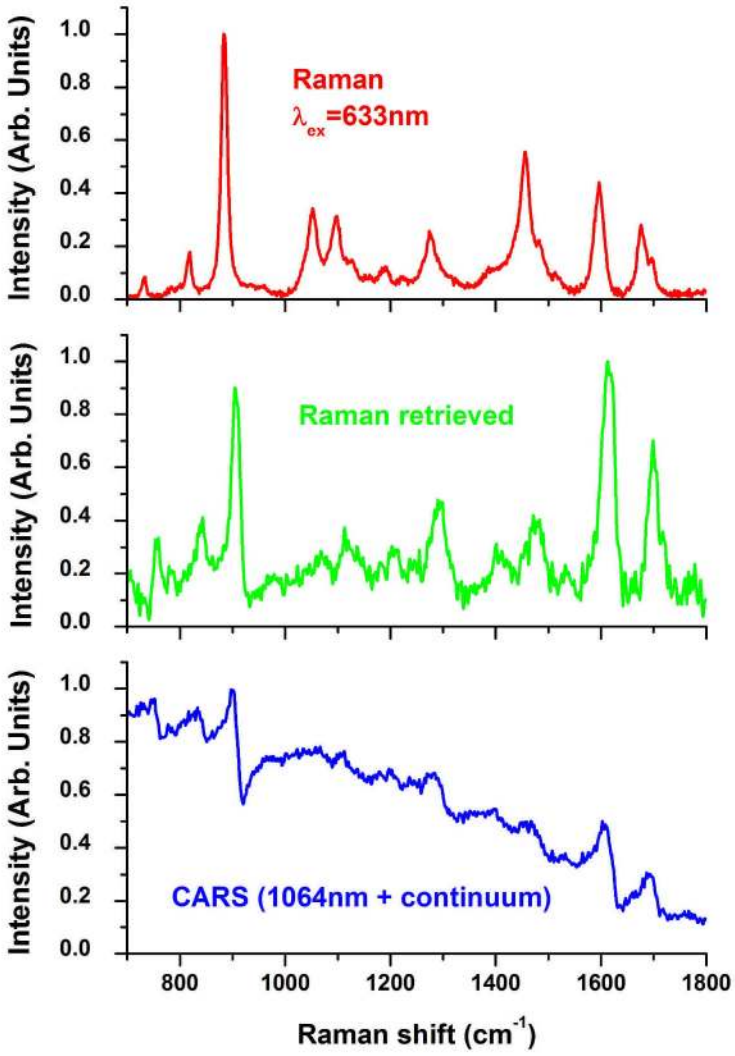

Figure 6.
Vibrational spectra of vanillin in isopropanol solution. Bottom panel: experimentally measured CARS spectrum (1064 nm and continuum excitation, 1064 nm probe). Middle panel: retrieved Raman spectrum. Top panel: experimentally measured spontaneous Raman spectrum (excitation wavelength 532 nm). The acquisition time for CARS spectrum was 100 times shorter than for spontaneous Raman. The incident powers were set at approximately the same level.

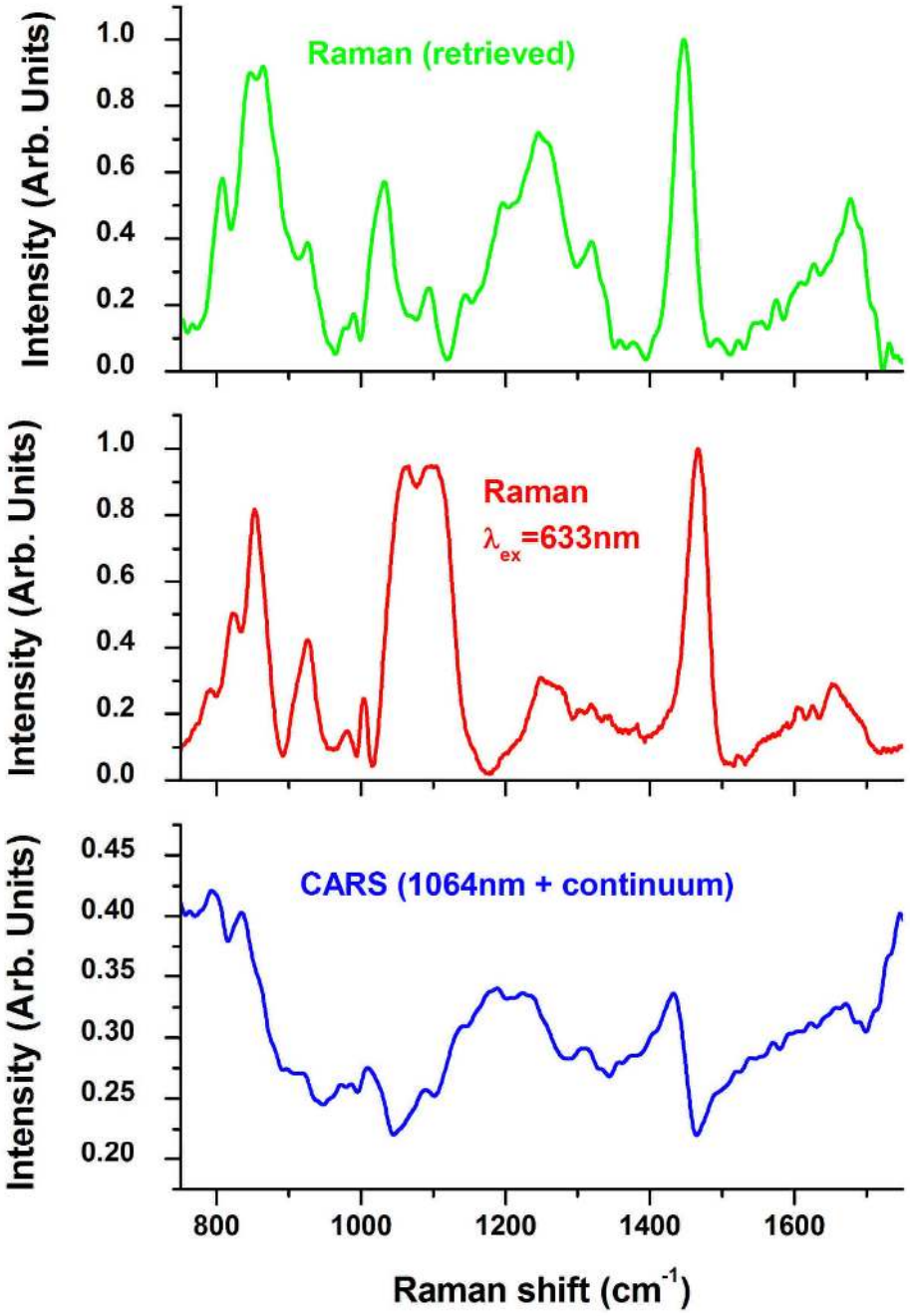

Figure 7.
Vibrational spectra of collagen-rich tissue. Bottom panel: experimentally measured CARS spectrum (1064 nm and continuum excitation, 1064 nm probe). Middle panel: experimentally measured spontaneous Raman spectrum. Top panel: retrieved Raman spectrum. The acquisition time for CARS spectrum was 100 times shorter than for spontaneous Raman. The incident powers were set at approximately the same level. Autofluorescence background was digitally subtracted from experimentally measured Raman spectrum.

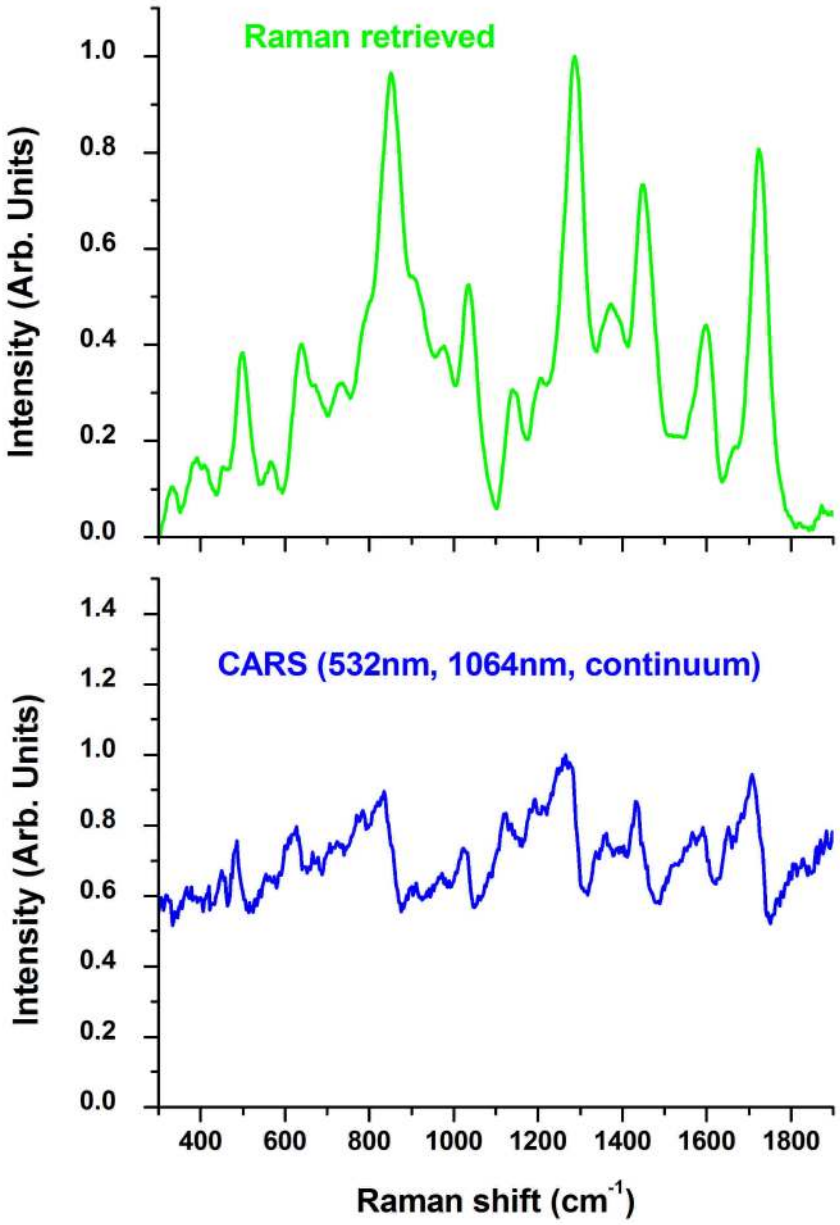

Figure 8.

Vibrational spectra of titania nanocrystals mixed with nail polish. Bottom panel: experimentally measured CARS spectrum (1064 nm and continuum excitation, probe pulse at 532 nm). Top panel: the retrieved Raman spectrum. Despite of a very large scattering of the sample and complex nature of the signal, the Raman lines corresponding to titania nanoparticles (at around 510 cm^{-1}, 640 cm^{-1}, 820 cm^{-1}) are clearly visible.

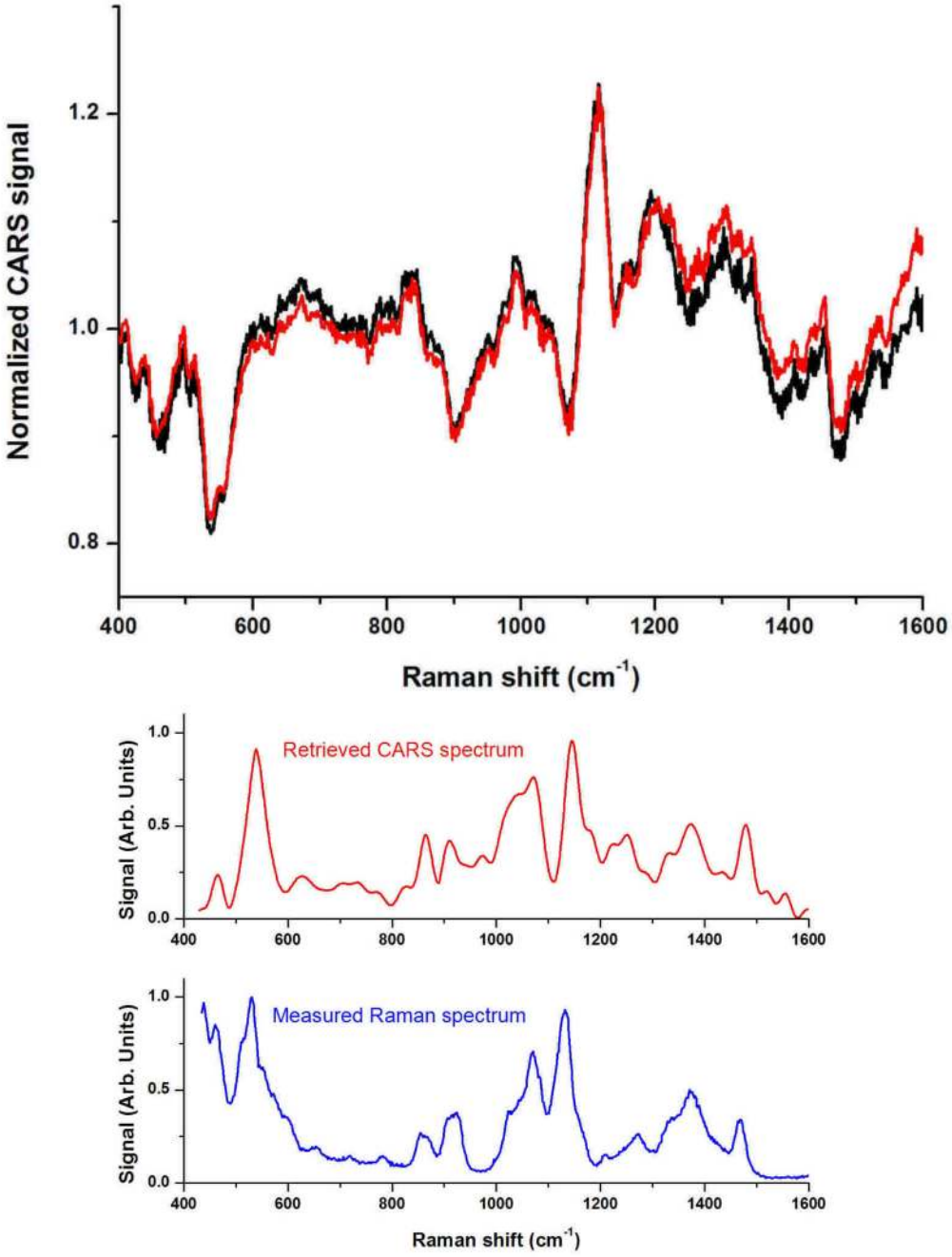

Figure 9.

Figure 9a. Typical CARS spectra from glucose solutions, showing spectra reproducibility for day-to-day operation. Black and red curves are CARS spectra from a buffer solution of glucose of slightly different concentrations (about 150 mg/dL). Spectra are shown on the same scale to emphasize the reproducibility.

Figure 9b. Top panel: Raman spectrum retrieved from the experimentally measured CARS spectrum (excitation wavelengths >1064nm); bottom panel: experimentally measured Raman spectrum (excitation wavelength 532nm). Glucose concentration is the same (150 mg/dL), and the incident average power is the same (50 mW). The CARS spectrum was collected within 1-s, while Raman spectrum took 100-s to collect. CARS spectrum was collected with a

thermoelectrically cooled CCD and spectral resolution 1 cm^{-1}, Raman spectrum was collected with liquid nitrogen cooled CCD and spectral resolution 5 cm^{-1}. Minor differences in spectral lines positions and their relative intensities are attributed to the very large difference in the incident wavelengths.